CHEMPHYSCHEM

DOI: 10.1002/cphc.201001067

Inelastic Neutron Scattering Study of Pt^{II} Complexes Displaying Anticancer Properties

Luís A. E. Batista de Carvalho,*[a] M. Paula M. Marques,[a, b] Christine Martin,[c] Stewart F. Parker,[d] and John Tomkinson[d]

The well-known platinum(II) chemotherapeutic drugs cisplatin [*cis*-$(NH_3)_2PtCl_2$] and carboplatin [$Pt(NH_3)_2C_6O_4H_6$], as well as the analogous transplatin [*trans*-$(NH_3)_2PtCl_2$], were studied by inelastic neutron scattering (INS) spectroscopy, coupled to quantum mechanical methods, and some ancillary work with X-ray diffraction on powders. An assignment of the experimental spectra was carried out based on the calculated INS transition frequencies and intensities (at the DFT level), thereby achieving a good correspondence between the calculated and observed data. Unusually good-quality INS spectra were obtained from about 250 mg, which is the smallest sample of a hydrogenous compound for which a successful INS interpretation has been reported. The knowledge of the local configuration of this kind of complexes is essential for an accurate understanding of their activity, which will pave the way for the rational design of novel third-generation drugs comprising cisplatin- and carboplatin-like moieties.

Introduction

Platinum-based antitumour drugs have been the target of intense research since Rosenberg's discovery of an unexpected inhibition of cell division in the presence of cisplatin, in the late sixties.[1] It is presently known that the antitumour properties of this type of compound—for example, cisplatin [*cis*-$(NH_3)_2PtCl_2$], still one of the most widely used anticancer drugs, and carboplatin [$Pt(NH_3)_2C_6O_4H_6$]—are based on selective interactions (DNA being their main biological target). They act by forming short-range intrastrand adducts with the cancer-cell DNA (mainly at the guanine–guanine, GG, and adenine–guanine, AG, base pairs), thus suppressing proliferation. However, they present several drawbacks, namely, severe toxicity and acquired resistance. Therefore, the search for structurally novel antitumour platinum compounds is crucial, aiming at the design of more efficient and less toxic agents. Polynuclear Pt^{II} complexes containing two or three metal centres and distinct aliphatic polyamines as bridging linkers, constitute a new class of third-generation drugs of great potential clinical importance.[2–4] In fact, this type of chelates can yield adducts containing long-distance intra- and interstrand crosslinks not available to the conventional mononuclear platinum complexes, their DNA binding properties being affected by simple structural changes. This enables to enhance DNA damage and achieve selective cytotoxicity through a rational design of these cisplatin- and carboplatin-like compounds.

Hence, studies of the local configuration of this kind of complexes make important contributions to understanding their activity. It is always preferable—wherever possible—to determine the structural parameters directly, usually via diffraction techniques. Carboplatin's crystal structure has been reported[5] and several crystallographic studies of *cis*-$Pt(NH_3)_2Cl_2$ are also found in the literature, but only one the lattice structure (the α-form) is clearly described.[6] Two other studies deal with the β-form, one indexed as a monoclinic structure[7] and the other as anorthic.[8] Regarding *trans*-$Pt(NH_3)_2Cl_2$, there is only one crystallographic study in the literature.[6] No phase transitions were noted in this isomer, probably because of the hydrogen bonding that can be inferred from the close intermolecular contact distances. However, no hydrogen atom positions have been determined for these structures, since they are not revealed by conventional crystal diffraction methods.

The absence of accurate structural information on the Pt^{II} chelates under study is due to the lack of good-quality crystals. Unfortunately, these compounds are very sensitive to preparative conditions and several forms are often stabilised in the powders produced, such that single crystals are not easily obtained. Indeed, structural defects are typically found in this broad class of inorganic systems, which leads to failure of conventional diffraction techniques. Under these circumstances, the alternative approach of vibrational spectroscopy offers some advantages, especially when modern ab initio calcula-

[a] *Dr. L. A. E. Batista de Carvalho, Dr. M. P. M. Marques*
Unidade I&D "Química-Física Molecular"
University of Coimbra, Rua Larga
3004-535 Coimbra (Portugal)
Fax: (+351) 239-826-541
E-mail: labc@ci.uc.pt

[b] *Dr. M. P. M. Marques*
Departamento de Ciências da Vida
University of Coimbra, Ap. 3046
3001-401 Coimbra (Portugal)

[c] *Dr. C. Martin*
CRISMAT, ENSICAEN, 6 Bd Ml Juin
14050 Caen Cedex (France)

[d] *Dr. S. F. Parker, Dr. J. Tomkinson*
ISIS Facility, STFC Rutherford Appleton Laboratory
Chilton, Didcot, OX11 0QX (United Kingdom)

tions can be exploited in order to generate the spectra of putative structures. In this respect, inelastic neutron scattering (INS) spectroscopy is the vibrational technique sine qua non. The spectral intensities [$S_i(Q^2, \nu_i)$] of the modes (i) can be quantitatively compared with those calculated, and the technique is particularly well suited to the study of hydrogenous compounds. Actually, the neutron scattering cross-section of an atom (σ) is characteristic of that atom and independent of the chemical environment. Since the value for hydrogen (80 barns) far exceeds that of all other atoms (typically ca. 5 barns), the modes of significant hydrogen displacement (u_i) dominate the INS spectra.[9] Then, for a mode at a given energy ν_i, the intensity from a powdered sample obeys the simplified relationship [Eq. (1)]:

$$S_i^{\bullet}(Q^2, \nu_i) = \frac{(Q^2 u_i^2)\,\sigma}{3} \exp\left(-\frac{Q^2 \alpha_i^2}{3}\right) \quad (1)$$

where Q (Å^{-1}) is the momentum transferred from the neutron to the sample and α_i (Å) is related to a weighted sum of all the displacements of the atom. Thus, not only the energies of the vibrational transitions (the eigenvalues, ν_i) but also the atomic displacements (the eigenvectors, u_i) are available from experimental observation. This significantly enhances the information obtainable from the vibrational technique and adds to that from the complementary Raman and infrared optical vibrational spectroscopic methods. By combining these results with quantum-mechanical molecular orbital calculations, it is possible to link molecular geometry with the experimental spectroscopic features and produce a reliable conformation for the systems under investigation.

Herein, we report an INS study of cisplatin, transplatin and carboplatin (Figure 1), coupled to X-ray powder diffraction (XRPD) experiments and quantum mechanical calculations (at the density functional theory, DFT, level). This is part of a broader research project aiming at a thorough conformational analysis of newly synthesised polynuclear polyamine Pt^{II} complexes. These comprise [$Pt(NH_3)_2Cl$] or [$Pt(NH_3)Cl_2$] cisplatin-like moities linked by alkanediamine chains of variable length, differing in the nature of the ligand and/or in the number and chemical environment of the metal centres. The final goal of these studies is the determination of the structure–activity relationships (SAR's) which underlie the antitumour properties of such compounds, which are concurrently being evaluated as to their antineoplastic activity towards human cancer cell lines.

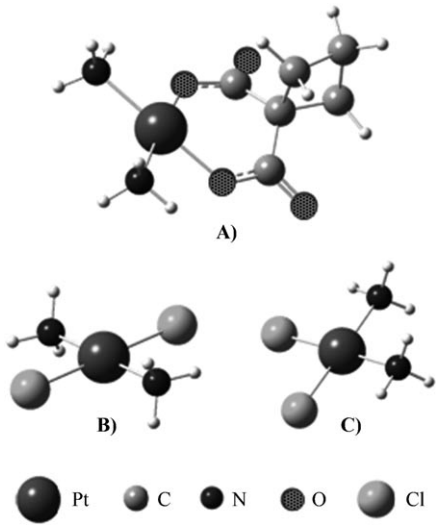

Figure 1. Calculated lowest-energy geometries for carboplatin (A), transplatin (B), and cisplatin (C) (mPW1PW/6-31G*/HW56 level of calculation).

Results and Discussion

The experimental INS spectra (below 1000 cm^{-1}) of cisplatin, transplatin and carboplatin are represented in Figure 2. The reported spectra refer principally to the motions of the hydrogenous ligands (NH_3 and cyclobutane ring). These modes, as will be shown below, always appear in the spectra, even for the smallest samples analysed, namely, 250 mg. We should emphasis here that this mass represents only 0.14 mmoles of hydrogen atoms and—to the best of our knowledge—it is the smallest sample of an hydrogenous compound for which a successful INS interpretation has been achieved so far. This offers considerable hope for the further development of the INS technique into the study of newly discovered drugs, for which only modest sample weights will be initially available (some early TOSCA work on C_{60} was undertaken on samples of about 0.7 mmoles, while the limiting sample mass for TOSCA work on dihydrogen is ca. 2 mmoles[10]).

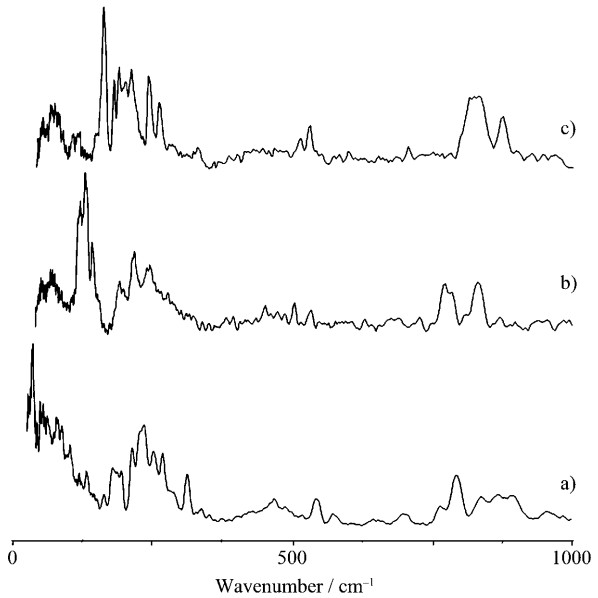

Figure 2. Experimental INS spectra (16–1000 cm^{-1}, at 20 K) for carboplatin (a), transplatin (b), and cisplatin (c).

For the Pt^{II} coordination compounds under study, the low energy spectra, below ≈550 cm^{-1}, can be conveniently discussed in terms of three general regions: the external mode interval including the whole body librations of the molecules, up to about 150 cm^{-1}; the ammonia region at about 200 cm^{-1}

(see below); and the skeletal deformation region. Above 550 cm^{-1}, local deformations of the ammonia ligand occur, the out-of-plane (ca. 780 cm^{-1}) and in-plane (ca. 830 cm^{-1}) rocking modes being the most obvious. The NH_3 internal deformations (both symmetric, at 1300–1350 cm^{-1}, and antisymmetric, at 1540–1650 cm^{-1}) and stretching vibrations (between 3200 and 3300 cm^{-1}), in turn, are more or less completely supressed as a result of the Debye–Waller factor, and will not be discussed here. This loss of spectral detail at higher frequencies is in line with similar effects previously seen in the INS spectra of the ammonium halides.[11]

The more straightforward cisplatin and transplatin systems will be considered first in this discussion. Above around 700 cm^{-1}, carefully chosen scaling factors[12] relate the mPW1 calculated transitions to features observed in the experimental vibrational spectra and the calculations are a ready guide to a reasonable assignment scheme (see Tables 1 and 2). Below 700 cm^{-1}, the mPW1 spectrum (as displayed in aCLIMAX) bears little or no relationship to that observed. Moreover, the lowest calculated bands (e.g. at $\approx$135 cm^{-1}) are much more intense than any observed feature below 500 cm^{-1}. These strong signals, easily identified from their calculated eigenvectors, are ascribed to the NH_3 torsional modes and their intensity comes from the large hydrogen displacements produced when this light mass oscillator undergoes torsion about the Pt–N bond. Significantly, light mass oscillators generate relatively intense overtones and combinations. This would nicely explain the broad intensity found between 280 and 490 cm^{-1}, assuming that the transitions calculated around 135 cm^{-1} correspond to those observed at about 150 to 240 cm^{-1}. Certainly, there are no fundamentals calculated at about 400 cm^{-1}. Such an assignment represents a significant shift of about 70 cm^{-1} for the NH_3 torsions in cisplatin.

This assignment scheme was modelled by creating two dummy vibrations, each for the two original ab initio ammonia torsions. The corresponding eigenvectors were chosen to be half those calculated for the original modes, and the eigenvalues adjusted to obtain a reasonable match with the observed spectra. To complete the assignment scheme (Table 1), the remaining bands had their eigenvalues scaled according to parameters previously developed by the authors.[12] This simple approach worked well on the cisplatin data, the correspondence between its calculated and observed INS spectra being evident in Figure 3.

The DMOL calculations, introducing the crystal lattice forces, produce the spectrum reported (unscaled) in Table 1. Whilst the mPW1 results for the NH_3 torsions are narrowly spread (but at too low an energy value), the DMOL results are too widely spread and display a poorer agreement with the experimental values. Those mPW1 features from 113 to 164 cm^{-1}, and the DMOL band at 300 cm^{-1}, must be assigned to the bulk of the scattering intensity from 160 to 230 cm^{-1} (see Figure 4). The remaining features in the DMOL spectrum align quite well with those observed, and refer mostly to external li-

Table 1. Experimental (INS and Raman) and calculated wavenumbers (below 1700 cm^{-1}) for cisplatin (C_{2v} symmetry).

Exp. INS	Exp. Raman[12]	Calc. DMOL	Calc. G03W[a]	Scaled G03W[b]	Sym. species[c]	Approximate description[d]
		31				external translation
		37				external translation
		67				external translation
~72		79				external libration (about N–Cl axis #1) in-phase
~90		91				external libration (about N–Cl axis #2) in-phase
		109				external libration (about N–Cl axis #1) out-of-phase
~125	120	123				external libration (vertical axis) in- and out-of-phase
		138				external libration (about N–Cl axis #2) out-of-phase
162	162	158	150	162	A_1	δ(Cl–Pt–Cl)
174		180	113	174	A_2	γ′(Cl–Pt–N)
192		265	139	191[e]	A_2	τ′(NH_3)
211	210	292		211		
200			134	201	B_1	τ(NH_3)
221		300		221[e]		
		212				γ(Cl–Pt–N)
~228		228	164	230	B_1	γ(Cl–Pt–N)
251	255	270	226	251	A_1	δ(Cl–Pt–N)
268		219	231	268	B_2	δ(Cl–Pt–N)
	317	314	338	321	B_2	ν_{as}(Cl–Pt–N) + τ(NH_3)
~330	323	325	349	332	A_1	ν_s(Cl–Pt–Cl)
505	508	536	465	516	B_2	ν_{as}(N–Pt–N)
521	524	555	472	524	A_1	ν_s(N–Pt–N)
778	724		760	783	A_2	r_γ(NH_3)
~790	789		779	802	B_1	r_γ(NH_3)
~808	811		790	813	B_2	r_β(NH_3)
845	824		825	849	A_1	r_β(NH_3)
1297	1295		1321		B_2	out-of-phase δ_s(NH_3)
1325	1316		1328		A_1	in-phase δ_s(NH_3)
~1540	1537		1682		B_2	δ_a(NH_3)
~1595	1601		1691		A_1	δ_a(NH_3)
			1714		A_2	δ_a(NH_3)
	1648		1721		B_1	δ_a(NH_3)

[a] mPW1PW/6-31G*/HW56 level of calculation. [b] According to ref. [12]. [c] Based on the isolated molecule description. [d] τ: torsion; δ: in-plane deformation; Γ: out-of-plane deformation; ν: stretching; r_γ: out-of-plane rocking; r_β: in-plane rocking; t: twisting; ω, wagging; α: scissoring. [e] Dummy vibration (see text).

Table 2. Experimental (INS and Raman) and calculated wavenumbers (below 1700 cm^{-1}) for transplatin (C_{2h} symmetry).

Exp. INS	Exp. Raman	Calc. DMOL	Calc. G03W[a]	Fitted G03W	Sym. species[b]	Approximate description[c]
		41				external translation
		50				external translation
~72		60				external translation
~72		77				external libration (about N–N axis) in-phase
~90		94				external libration (about vertical axis) in-phase
	91	95				external libration (about N–N axis) out-of-phase
~90		110				external libration (about vertical axis) out-of-phase
	124	139				external libration (about Cl–Cl axis) in-phase
138		178	57	137	A_u	$\tau(NH_3)_{out-of-phase}$
149				147[d]		
161	148	192	67	151	B_g	$\tau(NH_3)_{in-phase}$
				161[d]		
		147	135	138	B_u	δ(Cl–Pt–Cl) (Pt–N_2 translation)
		160				external libration (about Cl–Cl axis) out-of-phase
172		137	113	172	A_u	Γ(Cl–Pt–Cl) + $\tau(NH_3)_{out-of-phase}$
209	204	215	152	211	A_g	δ(N–Pt–Cl)
233		235	188	233	A_u	Γ(N–Pt–N)
259		248	223	258	B_u	δ(N–Pt–N)
	335	317	319	319	A_g	ν_s(Cl–Pt–Cl)
		320	337	337	B_u	ν_a(Cl–Pt–Cl)
514		510	498	514	B_u	ν_a(N–Pt–N)
542	539	530	535	542	A_g	ν_s(N–Pt–N)
775	781		772	775	B_g	$r_\gamma(NH_3)$ in-phase
790			809	790	A_g	$r_\beta(NH_3)$ in-phase
836			848	834	A_u	$r_\gamma(NH_3)$ out-of-phase
			869		B_u	$r_\beta(NH_3)$ out-of-phase
			1335		B_u	$\delta_s(NH_3)$ out-of-phase
	1299					
1304			1336		A_g	$\delta_s(NH_3)$ in-phase
	1313					
			1698		B_u	$\delta_a(NH_3)$
	1528		1700		A_g	$\delta_a(NH_3)$
~1650	1598		1700		B_g	$\delta_a(NH_3)$
			1701		A_u	$\delta_a(NH_3)$

[a] mPW1PW/6-31G*/HW56 level of calculation. [b] Based on the isolated molecule description. [c] τ: torsion; δ: in-plane deformation; Γ: out-of-plane deformation; ν: stretching; r_γ: out-of-plane rocking; r_β: in-plane rocking; t: twisting; ω, wagging; α: scissoring. [d] Dummy vibration (see text).

brational modes of the complex as a whole, which cannot be generated by an isolated molecule calculation.

The results for transplatin are not dissimilar. Thus, whilst the mPW1 calculations yield transitions at too low an energy (Table 2), the DMOL results lead to the correct spectral region but, again, to too widely spread features (Figure 4b). The calculated intense features are once more assigned to the region of strongest observed bands. The whole body librations—although they display their lowest calculated transitions (at the DMOL level) at the same energy values (79 cm^{-1} for cisplatin and 77 cm^{-1} for transplatin, see Table 1 and 2)—are extended over a wider range in transplatin. This is no doubt due, in part, to the lower moment of inertia of the librations about the Cl–Pt–Cl axes in cisplatin. However, the in-phase libration of this type is calculated at 139 cm^{-1} for transplatin, no higher than the highest energy libration of cisplatin. We may conclude that the intermolecular forces are weaker in transplatin than in cisplatin. This can be quantified by considering librations about the vertical axis through the Pt atom: 123 cm^{-1} for cisplatin and 97 cm^{-1} (average value) for transplatin. In fact, the moments of inertia should

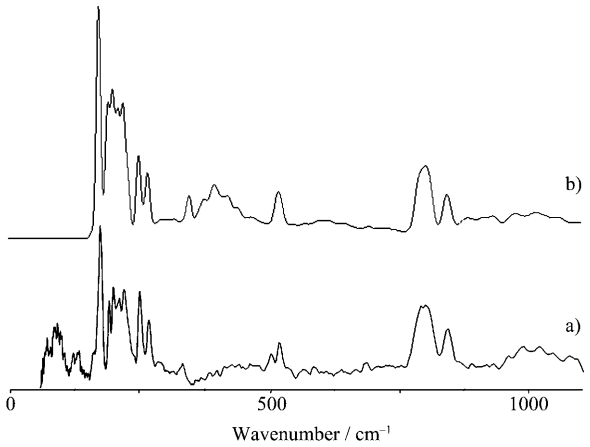

Figure 3. Experimental (a) and calculated (b) INS spectra (16–1100 cm^{-1}) for cisplatin.

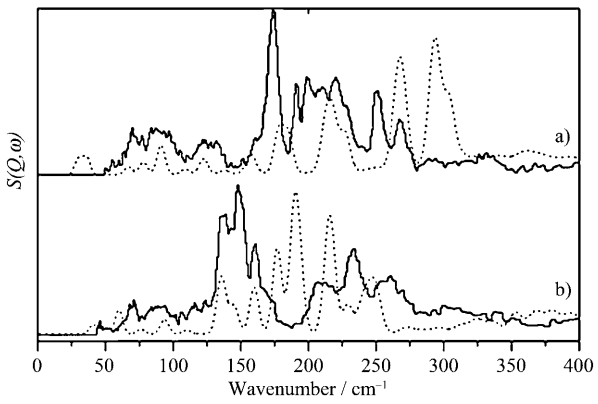

Figure 4. Comparison of experimental (——) and DMOL3-calculated (·····) INS spectra of cisplatin (a) and transplatin (b).

be very similar for these modes, for which only the intermolecular forces differ. According to the cisplatin structure, both NH_3 groups make contact with the same chlorine atom of the neighbouring molecule in the unit cell,[6] and as such there would be little difference between in-phase and out-of-phase librations of neighbouring molecules. In transplatin, in turn, the in-phase motions, involving less strain on the $Cl\cdots NH_3$ close contacts, are expected to appear at lower energies than the out-of-phase modes (compare Tables 1 and 2 and Figures 2, 3, and 5).

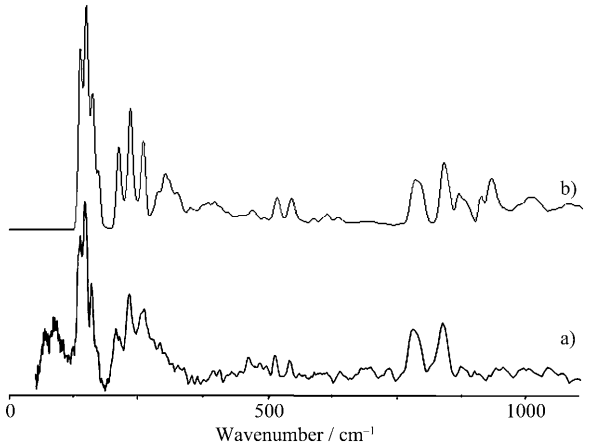

Figure 5. Experimental (a) and calculated (b) INS spectra (16–1100 cm^{-1}) for transplatin.

Even though X-ray powder diffraction is not the best method for the structural determination of this type of inorganic complexes, it is nevertheless remarkably sensitive to long-range order in these samples. The XRD pattern presently obtained from cisplatin shows the coexistence of at least two forms (Figure 6), which correspond to the α[6] and β[8] species

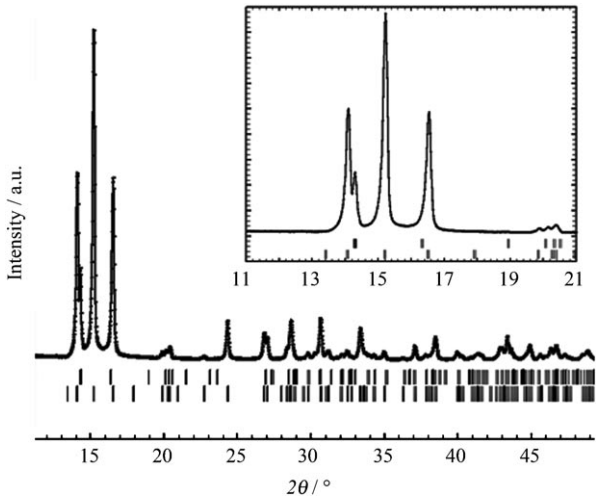

Figure 6. Experimental room-temperature XRD pattern for cisplatin. The upper and lower rows of tick-marks correspond to the phases α and β, respectively.

previously reported in the literature.[6–8] Unfortunately, the data is inadequate for a complete structural refinement of these forms. A single-crystal study would be necessary to elucidate the β cisplatin structure and fully characterise the differences between this and the α arrangement.

Finally, the more challenging carboplatin system will be discussed. The carboplatin molecule displays a *cis* arrangement of the two NH_3 moieties and a short distance between the carboxylate oxygens of the bidentate cyclobutanedicarboxylate ligand (Figure 1). Again, within the crystal structure, distinct hydrogen-bonding motifs were found,[5] but here they mostly represent a nearly three-dimensional network of contacts. There are four molecules to the unit cell, giving a total of eight librational modes, and consequently, even allowing for accidental degeneracy, the librational spectrum of the NH_3 groups should be rich. Moreover, the carbo ligand, also hydrogenous, is expected to give rise to clearly visible vibrations in the INS spectrum (Figure 7).

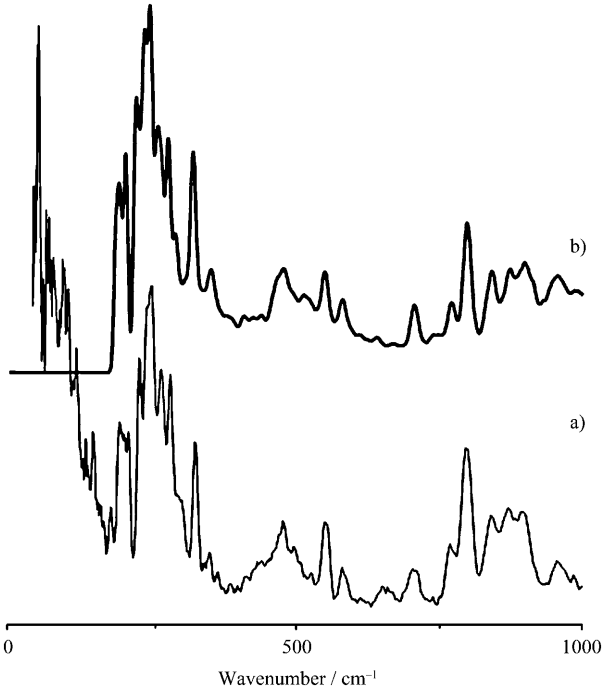

Figure 7. Experimental (a) and calculated (b) INS spectra (16–1000 cm^{-1}) for carboplatin.

The calculated INS features present at around 250 cm^{-1} for all the three Pt^{II} chelates studied herein (Figure 2), were compared (disregarding the contributions arising from the carbo moiety of carboplatin). It was verified that the calculated NH_3 torsional intensity at about 200 cm^{-1} approximately corresponds (in strength) to the intensity broadly observed around 250 cm^{-1} (Figures 3, 5, and 7). Based on this frequency shift (ca. 50 cm^{-1}), the assignment of these modes in carboplatin (Table 3) would nicely come into line with those of both cis- and transplatin. Again, this shift will also be due to N–H···O=C close contacts occurring in the crystal, which are responsible for a deepening of the wells corresponding to the ammonia li-

Table 3. Experimental (INS and Raman) and calculated wavenumbers (below 900 cm^{-1}) for carboplatin.

Exp. INS	Exp. Raman	Calc. G03W[a]	Fitted G03W	Approximate description[b]
	32			
~45	42			
	51			
~60	60			
	67			
~90				
97	93			
112	110			
141	137			
172				
187		46	186	"folding"[c]
		57	192	torsion[c]
196	192	76	196	"butterfly"[c]
203		118	204	cyclobutane "fan"[c]
222		149	220	cyclobutane "fan" + torsion[c]
		172	227	"folding" + $\tau(NH_3)$[c]
		174	234	$\tau(NH_3)$
~235	237	180	238	$\tau(NH_3)$
			[d]245	$\tau(NH_3)$
243	245		[d]247	$\tau(NH_3)$
		196	257	α(N–Pt–N) + $\tau(NH_3)$
260	262	198	265	α(N–Pt–N) + $\tau(NH_3)$
		218	276	Γ(C–O–Pt) + $\tau(NH_3)$
276		224	277	Γ(C–O–Pt) + $\tau(NH_3)$
~290	295	271	289	δ(O–Pt–O) + cyclobutane wagg
320	320	329	320	cyclobutane ring folding
	347	356	347	ν(Pt–O) + δ(C=O)
	353	366	353	ν(Pt–O) + δ(C=O)
		486	457	main ring breathing
~475	472	505	475	antisym main ring def
		463	546	ν_s(N–Pt–N)
548	546	465	548	ν_{as}(N–Pt–N)
580	572	569	580	sym main ring def + δ-(CCCC)
~705		670	705	r(CH_2) + δ(CCCC)
		716	770	Γ(C=O) out-of-phase
770	769	763	770	r(CH_2) + $r_\gamma(NH_3)$
		769	796	$r_\gamma(NH_3)$
796		782	798	$r_\gamma(NH_3)$
840	~835	814	840	r(CH_2) + $r_\beta(NH_3)$
		791	855	$r_\beta(NH_3)$
870	874	817	870	$r_\beta(NH_3)$
895		836	896	$r_\beta(NH_3)$
		874	896	r(CH_2) + $r_\beta(NH_3)$

[a] mPW1PW/6-31G*/HW56 level of calculation. [b] τ: torsion; δ: in-plane deformation; Γ: out-of-plane deformation; ν: stretching; r_γ: out-of-plane rocking; r_β: in-plane rocking; t: twisting; ω, wagging; α: scissoring. [c] According to Figure 8. [d] Dummy vibration (see text).

brations. A suitable adjustment of the carboplatin calculated spectrum was performed and a quite good agreement with the observed INS data was found (Figure 7). However, it is evident that the carboplatin feature below 150 cm^{-1} cannot be simply attributed to either the low-lying vibrational modes of the cyclobutane ligand, the external modes of the system, or any reasonable combination of the two. Rather, it is suggested that this spread of intensity stems from an increase in the local disorder introduced when the sample is quenched from ambient temperatures to the experimental conditions (20 K). This is supported by the crystal-structure determination, which showed an enhanced atomic disorder in the cyclobutane ring.[5] Indeed, it is likely that the disorder in the present sample is even greater than that of the crystal-structure determination. These local regions of disorder in the sample will lead directly to some fraction of the ammonia ligands being in irregular potential fields.

Finally, the combination of the INS spectra with the Raman spectra collected for the three Pt^{II} complexes investigated allowed a thorough assignment of their full vibrational pattern.

Conclusions

Herein, the INS spectra of three Pt^{II} chelates—transplatin and the chemotherapeutic agents cisplatin and carboplatin—were obtained. The fact that the extremely small amounts of sample used (ca. 250 mg) for this type of heavy-metal complexes still allowed the acquisition of good-quality data is rather hopeful for future INS studies of new compounds for which larger quantities may be initially unavailable.

The overall vibrational pattern of this kind of Pt^{II} chelates was found to be clearly dependent on their coordination geometry (e.g. *cis* or *trans* relative to the metal ion) and on the degree of covalent character of the metal–ligand bonds, as well as on the nature of the ligand. For the three complexes studied, a reasonable agreement was achieved between the experimental and calculated INS band positions. As expected, the modes associated to oscillators involved in intermolecular interactions (such as H-bonds, for example, Cl···H_3N), are not exactly reproduced by the calculations for the isolated molecule. In turn, they are well represented by the periodic DFT approach.

A rather straightforward approach for using the results from quantum mechanical molecular orbital calculations to interpret the experimental spectra was exploited. The calculated frequencies were found to be substantially improved by applying a scaling/fitting procedure to the mPW1 results. The full calculation of molecules in their lattice (DMOL results), in turn, was used unscaled. The agreement achieved between these and the experimental INS spectrum indicates that the calculated geometry is representative of the true crystalline form. The results for all the internal modes below about 1000 cm^{-1} were found to be in agreement with Raman studies performed by the authors for these and for similar systems, as well as with reported experimental[13] and calculated[14,15] data on several dihalodiammine Pt^{II} complexes.

The knowledge yielded by this type of work—together with concurrent experiments carried out in distinct human cancer cells (in vitro assessment of growth-inhibition properties and effect on the metabolic profile)[16–22]—should help expose the molecular basis of toxicity, with a view to rationally designing new and more effective anticancer agents for future clinical use.

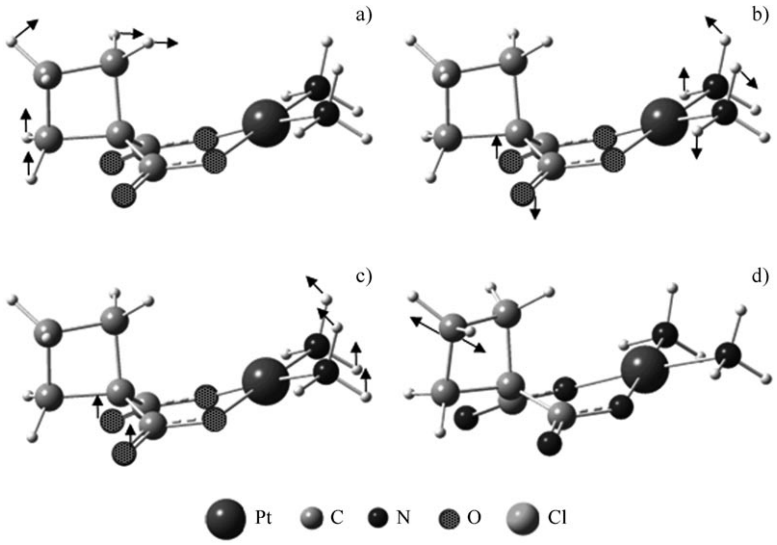

Figure 8. Schematic representation of the low-frequency vibrational modes for carboplatin: "folding" (a), "torsion" (b), "butterfly" (c), and cyclobutane "fan" (d).

Experimental Section

INS Spectroscopy: INS spectra were obtained in the Rutherford Appleton Laboratory (UK), at the ISIS pulsed neutron source, on the TOSCA spectrometer. This is an indirect geometry time-of-flight, high resolution [($\Delta E/E$) ca. 1.25%], broad range spectrometer.[9] The samples, Sigma–Aldrich (99.9+ %), weighing 250–300 mg, were wrapped in aluminium foil. To reduce the impact of the Debye–Waller factor [the exponential in Eq. (1)] on the observed spectral intensity, the samples were cooled to about 20 K. The data were recorded in the energy range 16–4000 cm^{-1} and converted to the conventional scattering law, S(Q, ν) versus energy transfer (in cm^{-1}) through standard programs.[9]

X-ray Powder Diffraction: XRPD data were measured at room temperature in an X'Pert Philips diffractometer (Cu Kα radiation) from 10 to 90° and in the 2θ range. The data were analysed using the Fullprof suite.[23]

Quantum Mechanical Calculations: The quantum mechanical calculations (full geometry optimisation and calculation of the harmonic vibrational frequencies) were performed using the GAUSSIAN 03W program (G03W),[24] within the DFT approach, in order to properly account for the electron correlation effects (particularly important in this kind of systems). The mPW1PW method, which comprises a modified version of the exchange term of Perdew–Wang and the the Perdew–Wang 91 correlation functional,[25,26] was used, along with the split valence basis set 6–31G*,[27] for all atoms except for the metal. Pt^{II} was represented by the relativistic effective core potentials (ECPs) of Hay and Wadt[28] (G03W keyword LANL2DZ), $n=5$ and $n=6$ being considered as valence electron shells. This DFT/ECP combination was found to be the best choice for describing cDDP,[12,29] since it presents the finest compromise between accuracy and computational demands. Results from these calculations will be referred to as 'mPW1'.

The molecular geometries were fully optimised by the Berny algorithm, using redundant internal coordinates: the bond lengths (to within about 0.1 pm) and the bond angles (to within ca. 0.1°). The final root-mean-square (rms) gradients were always less than 3×10^{-4} hartree $bohr^{-1}$ or hartree $radian^{-1}$. No geometrical constraints were imposed on the isolated molecules under study.

The complete unit cell of the compounds was also investigated with the periodic DFT code DMOL^3, as implemented in the Materials Studio package from Accelerys.[30] The generalised gradient approximation was used with a localised basis set (DNP double numerical with polarisation functions on all atoms including hydrogen), represented as a numerical tabulation, coupled to the Perdew and Wang[31] (PW91) functional. In each case, the published crystal structure was used as the starting structure.[5,6] Since the hydrogen atoms were not located in the X-ray structures, they were added at chemically reasonable positions. DMOL^3 performs geometry optimisations but not lattice optimisations. The vibrational spectra were calculated in the harmonic approximation from the energy-minimised structure, using the finite displacement technique to obtain the dynamical matrix. Starting from an energy-minimised geometry, each of the atoms in the unit cell was displaced by 0.005 Å in turn along the three Cartesian directions and a single-point calculation yielded the Hellman–Feynmann forces on all the atoms, from which the force constants were obtained by dividing by the corresponding displacement. Positive and negative displacements were used to obtain more accurate central finite differences. The force constant matrix F was transformed to mass-dependent coordinates by the G matrix, to give the dynamical matrix. Diagonalisation of the latter yielded the vibrational eigenvalues and eigenvectors.

The theoretical INS transition intensities were obtained from the calculated normal-mode eigenvectors of the quantum mechanical calculations, and the spectra simulated using the dedicated aCLIMAX program.[32] For isolated molecule calculations, this program accomodates the impact of the external modes of extended molecular solids through the choice of a suitable value for α_i (in the program this is the 'A-external' parameter and takes the values of 0.025 $Å^2$ in cisplatin, 0.040 $Å^2$ in transplatin, and 0.050 $Å^2$ in carboplatin). For periodic calculations, this procedure is not necessary since all the modes, both internal and external, are calculated.

Acknowledgements

This work was supported by the European Community through "Access to the Research Infrastructure Action of the Improving Human Potential Programme for ISIS Neutrons" (group leaders of Project n° 3-TOSCA RB13188). LAEBC and MPMM acknowledge financial support from the Portuguese Foundation for Science and Technology—Project PTDC/QUI/66701/2006 (co-financed by the European Community fund FEDER). The Rutherford Appleton Laboratory is thanked for access to neutron beam facilities.

Keywords: anticancer drugs · density functional calculations · inelastic neutron scattering · platinum · X-ray diffraction

[1] B. Rosenberg, L. Van Camp, J. E. Trosko, V. H. Mansour, *Nature* **1969**, *222*, 385.
[2] N. Farrell in *Platinum-based Drugs in Cancer Therapy* (Eds.: L. R. Kelland, N. P. Farrell), Humana Press Inc, Totowa, **2000**, pp. 321 – 338, and references therein.
[3] C. Mitchell, P. Kabolizadeh, J. Ryan, J. D. Roberts, A. Yacoub, D. T. Curiel, P. B. Fisher, M. P. Hagan, N. P. Farrell, S. Grant, P. Dent, *Mol. Pharmacol.* **2007**, *72*, 704.
[4] A. Hegmans, J. Kasparkova, O. Vrana, L. R. Kelland, V. Brabec, N.P Farrell, *J. Med. Chem.* **2008**, *51*, 2254.
[5] a) S. Neidle, I. M. Ismail, P. J. Sadler, *J. Inorg. Biochem.* **1980**, *13*, 205; b) B. Beagley, D. W. J. Cruickshank, C. A. McAuliffe, R. G. Pritchard, A. M. Zaki, R. L. Beddoes, R. J. Cernik, O. S. Mills, *J. Mol. Struct.* **1985**, *130*, 97.
[6] G. H. W. Milburn, M. R. Truter, *J. Chem. Soc. A* **1966**, 1609; ICDD 25–0611 (M. M.Yevitz, J. A. Stanko).
[7] ICDD 50–0643 (M. M.Yevitz, J. A. Stanko).
[8] ICDD 50–0643 (S. Kirik, L. Solovyev, A. Blokhin, R. Mulagaleev).
[9] P. C. H. Mitchell, S. F. Parker, A. J. Ramirez-Cuesta, J. Tomkinson in *Vibrational Spectroscopy with Neutrons, Series on Neutron Techniques and Applications, Vol. 3* (Eds.: J. L. Finney, D. L. Worcester), World Scientific Press, **2005**.
[10] P. C. H. Mitchell, A. J. Ramirez-Cuesta, S. F. Parker, J. Tomkinson, D. Thompsett, *J. Phys. Chem. B* **2003**, *107*, 6838.
[11] J. Tomkinson, G. J. Kearley, *J. Chem. Phys.* **1989**, *91*, 5164.
[12] A. M. Amado, S. M. Fiuza, M. P. M. Marques, L. A. E. Batista de Carvalho, *J. Chem. Phys.* **2007**, *127*, 185104.
[13] a) K. Nakamoto, P. J. McCarthy, J. Fujita, R. A. Condrate, G. T. Behnke, *Inorg. Chem.* **1965**, *4*, 36; b) R. H. Perry, D. P. Athans, E. F. Young, J. R. Durig, B. R. Mitchell, *Spectrochim. Acta Part A* **1967**, *23*, 1137; c) I. A. Degen, A. J. Rowlands, *Spectrochim. Acta Part A* **1991**, *47*, 1263; d) H. Baranska, J. Kuduk-Jaworska, S. Cacciari, *J. Raman Spectrosc.* **1997**, *28*, 1.
[14] P. V. N. Pavankumar, P. Seetharamulu, S. Yao, J. D. Saxe, D. G. Reddy, F. H. Hausheer, *J. Comput. Chem.* **1999**, *20*, 365.
[15] L. Zhang, H. Wei, Y. Zhang, Z. Guo, L. Zhu, *Spectrochim. Acta Part A* **2002**, *58*, 217.
[16] M. P. M. Marques, M. T. Girão da Cruz, M. C. Pedroso de Lima, A. Gameiro, E. Pereira, P. Garcia, *Biochim. Biophys. Acta Mol. Cell Res.* **2002**, *1589*, 63.
[17] L. J. Teixeira, M. Seabra, E. Reis, M. T. Girão da Cruz, M. C. Pedroso de Lima, E. Pereira, M. A. Miranda, M. P. M. Marques, *J. Med. Chem.* **2004**, *47*, 2917.
[18] A. S. Soares, S. M. Fiuza, M. J. Gonçalves, L. A. E. Batista de Carvalho, M. P. M. Marques, A. M. Urbano, *Lett. Drug Des. Discovery* **2007**, *4*, 460.
[19] O. Corduneanu, A. M. Chiorcea-Paquim, V. Diculescu, S. M. Fiuza, M. P. M. Marques, A. M. Oliveira-Brett, *Anal. Chem.* **2010**, *82*, 1245.
[20] A. Tassoni, N. Bagni, M. Ferri, M. Franceschetti, A. Khomutov M. P. M. Marques, S. M. Fiuza, A. R. Simonian, D. Serafini-Fracassini, *Plant Physiol. Biochem.* **2010**, *48*, 496.
[21] R. Tummala, P. Diegelman, S. M. Fiuza, L. A. E. Batista de Carvalho, M. P. M. Marques, D. L. Kramer, K. Clark, S. Vujcic, C. W. Porter, L. Pendyala, *Oncol. Rep.* **2010**, *24*, 15.
[22] I. F. Duarte, I. Lamego, J. Marques, M. P. M. Marques, B. J. Blaise, A. M. Gil, *J. Proteome Res.* **2010**, *9*, 5877.
[23] http://www.ill.eu/instruments-support/useful-tools/fullprof/.
[24] *Gaussian 03 (Revision B.04)*, M. J. Frisch, G. W. Trucks, H. B. Schlegel, G. E. Scuseria, M. A. Robb, J. R. Cheeseman, J. A. Montgomery, Jr., T. Vreven, K. N. Kudin, J. C. Burant, J. M. Millam, S. S. Iyengar, J. Tomasi, V. Barone, B. Mennucci, M. Cossi, G. Scalmani, N. Rega, G. A. Petersson, H. Nakatsuji, M. Hada, M. Ehara, K. Toyota, R. Fukuda, J. Hasegawa, M. Ishida, T. Nakajima, Y. Honda, O. Kitao, H. Nakai, M. Klene, X. Li, J. E. Knox, H. P. Hratchian, J. B. Cross, C. Adamo, J. Jaramillo, R. Gomperts, R. E. Stratmann, O. Yazyev, A. J. Austin, R. Cammi, C. Pomelli, J. W. Ochterski, P. Y. Ayala, K. Morokuma, G. A. Voth, P. Salvador, J. J. Dannenberg, V. G. Zakrzewski, S. Dapprich, A. D. Daniels, M. C. Strain, O. Farkas, D. K. Malick, A. D. Rabuck, K. Raghavachari, J. B. Foresman, J. V. Ortiz, Q. Cui, A. G. Baboul, S. Clifford, J. Cioslowski, B. B. Stefanov, G. Liu, A. Liashenko, P. Piskorz, I. Komaromi, R. L. Martin, D. J. Fox, T. Keith, M. A. Al-Laham, C. Y. Peng, A. Nanayakkara, M. Challacombe, P. M. W. Gill, B. Johnson, W. Chen, M. W. Wong, C. Gonzalez, J. A. Pople, Gaussian Inc., Pittsburgh PA, USA, **2003**.
[25] C. Adamo, V. Barone, *J. Chem. Phys.* **1998**, *108*, 699.
[26] J. P. Perdew, K. Burke, Y. Wang, *Phys. Rev. B* **1996**, *54*, 16533.
[27] P. C. Hariharan, J. A. Pople, *Theor. Chim. Acta* **1973**, *28*, 213.
[28] P. J. Hay, W. R. Wadt, *J. Chem. Phys.* **1985**, *82*, 299.
[29] S. M. Fiuza, A. M. Amado, M. P. M. Marques, L. A. E. Batista de Carvalho, *J. Phys. Chem. A* **2008**, *112*, 3253.
[30] B. Delley, *J. Chem. Phys.* **2000**, *113*, 7756.
[31] J. P. Perdew, Y. Wang, *Phys. Rev. B* **1992**, *45*, 13244.
[32] A. J. Ramirez-Cuesta, *Comput. Phys. Commun.* **2004**, *157*, 226.

Received: December 22, 2010
Revised: March 11, 2011

